

of CENP-E stepping on the resisting force was similar on these two lattices. The average dwell time between the steps for the entire force range was also similar on T- and D-MTs (fig. S9G). We further observed a slightly shorter dwell time at low force on D-MTs, which is consistent with the faster velocity of CENP-E walking on this type of microtubules (Fig. 2G). CENP-E responded to larger loads by lengthening its dwells on D-MTs, but not on T-MTs. Under the load, CENP-E also detached less frequently from D-MTs (Fig. 2H). As a result, the peak force for CENP-E detachment was shifted to significantly higher values on D-MTs (Fig. 2I), indicating that the effect of tubulin dettyrosination is exerted mostly on CENP-E detachment, rather than stepping. Thus, CENP-E can carry a significantly larger load on D-MTs *in vitro*.

Our data support a model in which CENP-E-dependent transport of pole-proximal chromosomes toward the spindle equator requires microtubule tracks that are dettyrosinated. Therefore, increasing tubulin dettyrosination should disrupt the biased motion of pole-proximal chromosomes toward the equator and cause their delivery to inappropriate cellular locations. To test this, we increased tubulin dettyrosination by depleting TTL by means of RNA interference (RNAi) in U2OS cells (fig. S10A). TTL depletion caused ubiquitous dettyrosination of spindle microtubules (including astral microtubules) during early mitosis (fig. S10B) (27). Of TTL-depleted cells, 65% delayed mitotic progression and failed to congress all the chromosomes (Fig. 3A and movie S5). In these cells, the pole-proximal chromosomes did not remain stuck at the spindle poles, as observed after CENP-E inhibition or after blocking tubulin dettyrosination, but were transported in various directions, including toward the cell cortex (Fig. 3, A and B). This suggests that the spatial cues that normally guide CENP-E toward the equator were disrupted. CENP-E inhibition in live TTL-depleted cells significantly decreased the transport of chromosomes away from spindle poles (Fig. 3, A and B). This was confirmed in a large population of fixed cells by use of a quantitative monopolar spindle configuration assay (Fig. 4, A to C) (I), indicating that the random transport of chromosomes along ubiquitously dettyrosinated spindle microtubules after TTL RNAi is mediated by CENP-E.

Taken together, our work establishes the specific molecular mechanism that guides CENP-E-dependent chromosome motion toward the cell equator. This mechanism is based on the ability of CENP-E to transport pole-proximal chromosomes preferentially on dettyrosinated microtubule tracks, which are normally oriented toward the spindle equator (fig. S11). We propose that microtubule dettyrosination works as a navigation system that guides kinetochore motors during cell division, ultimately contributing to faithful chromosome segregation.

REFERENCES AND NOTES

1. M. Barisic, P. Aguiar, S. Geley, H. Maiato, *Nat. Cell Biol.* **16**, 1249–1256 (2014).
2. T. M. Kapoor *et al.*, *Science* **311**, 388–391 (2006).

3. C. E. Walczak, S. Cai, A. Khodjakov, *Nat. Rev. Mol. Cell Biol.* **11**, 91–102 (2010).
4. P. Kalab, R. Heald, *J. Cell Sci.* **121**, 1577–1586 (2008).
5. T. Kiyomitsu, I. M. Cheeseman, *Nat. Cell Biol.* **14**, 311–317 (2012).
6. Y. Kim, A. J. Holland, W. Lan, D. W. Cleveland, *Cell* **142**, 444–455 (2010).
7. J. Whyte *et al.*, *J. Cell Biol.* **183**, 819–834 (2008).
8. S. Cai, C. B. O'Connell, A. Khodjakov, C. E. Walczak, *Nat. Cell Biol.* **11**, 832–838 (2009).
9. K. J. Verhey, J. Gaertig, *Cell Cycle* **6**, 2152–2160 (2007).
10. C. Janke, *J. Cell Biol.* **206**, 461–472 (2014).
11. G. G. Gundersen, J. C. Bulinski, *J. Cell Biol.* **102**, 1118–1126 (1986).
12. P. J. Wilson, A. Forer, *Cell Motil. Cytoskeleton* **14**, 237–250 (1989).
13. G. G. Gundersen, M. H. Kalnoski, J. C. Bulinski, *Cell* **38**, 779–789 (1984).
14. N. A. Reed *et al.*, *Curr. Biol.* **16**, 2166–2172 (2006).
15. Y. Konishi, M. Setou, *Nat. Neurosci.* **12**, 559–567 (2009).
16. J. W. Hammond *et al.*, *Mol. Biol. Cell* **21**, 572–583 (2010).
17. M. Sirajuddin, L. M. Rice, R. D. Vale, *Nat. Cell Biol.* **16**, 335–344 (2014).
18. K. Ersfeld *et al.*, *J. Cell Biol.* **120**, 725–732 (1993).
19. X. Fonrose *et al.*, *Cancer Res.* **67**, 3371–3378 (2007).
20. I. Poser *et al.*, *Nat. Methods* **5**, 409–415 (2008).
21. T. J. Yen, G. Li, B. T. Schaar, I. Szilak, D. W. Cleveland, *Nature* **359**, 536–539 (1992).
22. Materials and methods are available as supplementary materials on Science Online.
23. N. Gudimchuk *et al.*, *Nat. Cell Biol.* **15**, 1079–1088 (2013).
24. H. Yardimci, M. van Duffelen, Y. Mao, S. S. Rosenfeld, P. R. Selvin, *Proc. Natl. Acad. Sci. U.S.A.* **105**, 6016–6021 (2008).
25. N. J. Carter, R. A. Cross, *Nature* **435**, 308–312 (2005).
26. M. Nishiyama, H. Higuchi, T. Yanagida, *Nat. Cell Biol.* **4**, 790–797 (2002).
27. L. Peris *et al.*, *J. Cell Biol.* **174**, 839–849 (2006).

ACKNOWLEDGMENTS

We thank F. I. Ataullakhanov for help with the laser trap and data analysis; A. Kiyatkin, V. Mustyatsa, M. Molodtsov, A. Gautreau, G. Lakisic, and M. Barisic for technical assistance; and members of

our laboratories for stimulating discussions. This work was supported by National Institutes of Health grant R01-GM098389 and RSG-14-018-01-CCG from the American Cancer Society to E.L.G.; by the Institut Curie, the Centre National de la Recherche Scientifique, the Institut National de la Santé et de la Recherche Médicale, the L'Agence Nationale de la Recherche (ANR) award ANR-12-BSV2-0007, INCA_6517, ANR-10-LBX-0038, part of the IDEX Idex PSL, ANR-10-IDEX-0001-02 PSL to C.J.; and Fundação Luso-Americana para o Desenvolvimento (FLAD) Life Science 2020 and PRECISE grant from the European Research Council to H.M. A.V.Z. is supported by the RAS Presidium Grants "Mechanisms of the Molecular Systems Integration," "Molecular and Cell Biology programs," and Russian Fund for Basic Research Grant 12-04-00111-a and 13-00-40188. R.S.S. is supported by a fellowship from the Programa Graduado em Áreas da Biologia Básica e Aplicada (GABBA) PhD program from the University of Porto. A.L.P. is supported by fellowship SFRH/BPD/66707/2009 from Fundação para a Ciência e a Tecnologia of Portugal. M.B., R.S.S., S.K.T., M.M.M., C.J., E.L.G., and H.M. designed the experiments; M.B. performed all experiments in cells; M.M.M. established and performed the tubulin purification protocol from HeLa cells; R.S.S. performed single-molecule experiments; S.K.T. performed force measurements; A.L.P. provided reagents; all authors analyzed data; H.M., E.L.G., and M.B. wrote the paper, with contributions from all authors; H.M. conceived and coordinated the project. Data described can be found in the main figures and supplementary materials. The authors declare no conflict of interests.

SUPPLEMENTARY MATERIALS

www.sciencemag.org/content/348/6236/799/suppl/DC1
Materials and Methods

Figs. S1 to S12

Table S1

References (28–43)

Movies S1 to S5

17 December 2014; accepted 9 April 2015

Published online 23 April 2015;

10.1126/science.125175

CANCER IMMUNOTHERAPY

A dendritic cell vaccine increases the breadth and diversity of melanoma neoantigen-specific T cells

Beatriz M. Carreno,^{1*} Vincent Magrini,² Michelle Becker-Hapak,¹ Saghar Kaabinejadian,³ Jasreet Hundal,² Allegra A. Petti,² Amy Ly,² Wen-Rong Lie,⁴ William H. Hildebrand,³ Elaine R. Mardis,² Gerald P. Linette¹

T cell immunity directed against tumor-encoded amino acid substitutions occurs in some melanoma patients. This implicates missense mutations as a source of patient-specific neoantigens. However, a systematic evaluation of these putative neoantigens as targets of antitumor immunity is lacking. Moreover, it remains unknown whether vaccination can augment such responses. We found that a dendritic cell vaccine led to an increase in naturally occurring neoantigen-specific immunity and revealed previously undetected human leukocyte antigen (HLA) class I–restricted neoantigens in patients with advanced melanoma. The presentation of neoantigens by HLA-A*02:01 in human melanoma was confirmed by mass spectrometry. Vaccination promoted a diverse neoantigen-specific T cell receptor (TCR) repertoire in terms of both TCR- β usage and clonal composition. Our results demonstrate that vaccination directed at tumor-encoded amino acid substitutions broadens the antigenic breadth and clonal diversity of antitumor immunity.

Melanoma genomes harbor somatic mutations that are caused by exposure to mutagens such as ultraviolet light (1, 2). Tumor missense mutations, translated into amino acid substitutions (AASS), may

provide a form of antigens that the immune system perceives as foreign, which in turn elicits tumor-specific T cell immunity (3–6). To examine the immunogenicity of tumor-encoded AASS, we obtained the consent of three patients with

stage III resected cutaneous melanoma (MEL21, MEL38, and MEL218) for genomic analysis of their surgically excised tumors. The three patients were then enrolled in a phase I clinical trial with autologous, functionally mature, interleukin-12p70 (IL-12p70)-producing dendritic cell vaccine (fig. S1) (7). All three patients had received prior treatment with ipilimumab (see supplementary materials). Exome sequencing was performed to identify somatic mutations in tumor samples (Fig. 1A). Multiple metachronous tumors were analyzed from patients MEL21 and MEL38 (tables S1 and S2). Tumor missense mutations, translated as AAS-encoding nonamer peptides, were filtered

through in silico analysis to assess HLA-A*02:01 peptide-binding affinity (8), and expression of genes encoding predicted HLA-A*02:01 peptide candidates was determined by analysis of cDNA capture data (Fig. 1A) (9). Peptide candidates for experimental validation were selected according to the strategy described in fig. S2; HLA-A*02:01 binding was evaluated using the T2 assay (fig. S3) (10) and confirmed with the fluorescence polarization-based competitive peptide-binding assay of Buchli *et al.* (11). Seven AAS peptide candidates per patient were selected from validated HLA-A*02:01 binders (fig. S2 and table S4) for incorporation into a personalized vaccine formulation, along with the melanoma gp100-derived peptides G209-2M and G280-9V as positive controls for vaccination (7). The expression pattern of mutated genes encoding vaccine candidates is shown in Venn diagrams in Fig. 1A.

To examine the kinetics and magnitude of T cell immunity to AAS peptides upon vaccination, we collected peripheral blood mononuclear cells

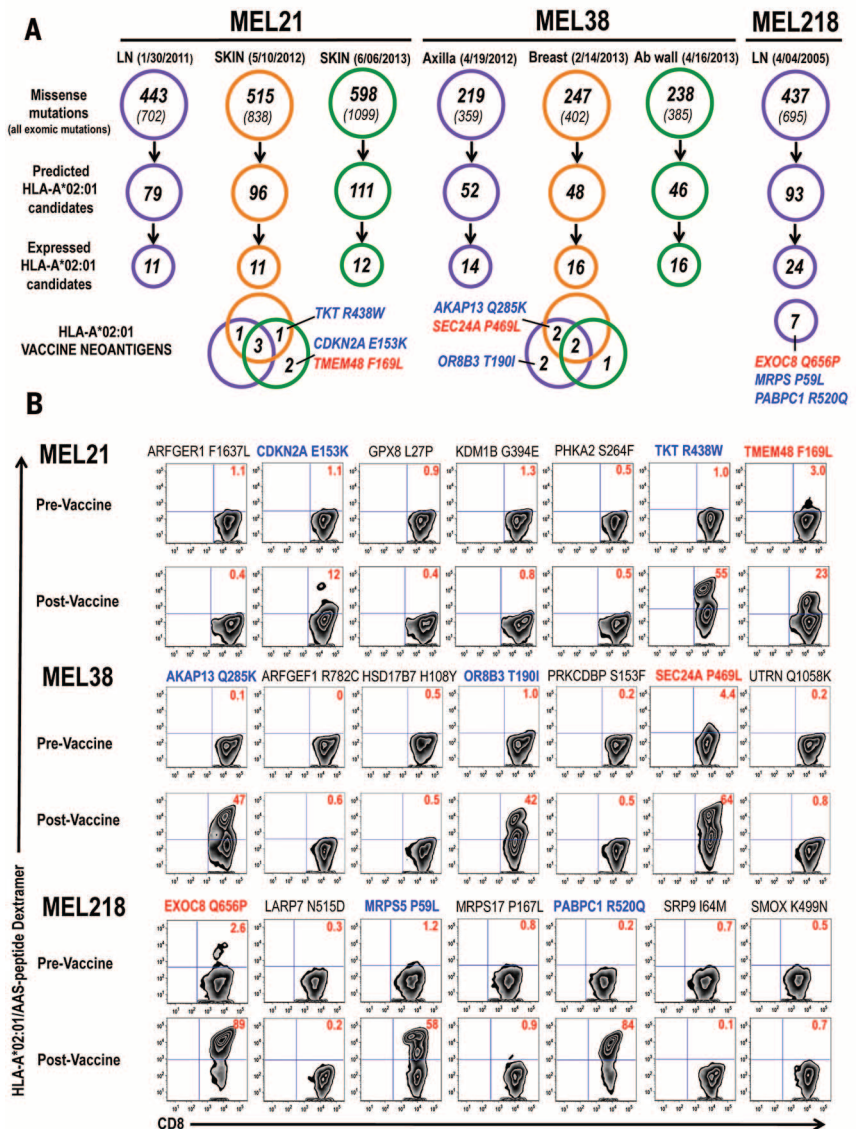
(PBMCs) prior to vaccination and weekly thereafter. The CD8⁺ T cell response to each peptide was analyzed using a HLA-A*02:01/AAS-peptide dextramer assay after a single round of in vitro stimulation (fig. S4A) (7). Immune monitoring demonstrated that in each patient, T cell immunity to one AAS peptide could be detected in prevaccine PBMC samples after in vitro stimulation (MEL21, TMEM48 F169L; MEL38, SEC24A P469L; MEL218, EXOC8 Q656P) (Fig. 1B), although not directly from the blood (fig. S4B). Preexisting immunity to these three neoantigens was confirmed in ex vivo expanded, prevaccine-purified CD8⁺ T cells by means of dextramer assay (fig. S4B) and interferon (IFN)- γ production (12) (fig. S4C).

Vaccination augmented the T cell response to these neoantigens, with observed frequencies of 23% TMEM48 F169L⁺ CD8⁺ T cells, 64% SEC24A P469L⁺ CD8⁺ T cells, and 89% EXOC8 Q656P⁺ CD8⁺ T cells detected upon culture at the peak of response (Fig. 1B). Immune monitoring also

¹Department of Medicine, Division of Oncology, Washington University School of Medicine, St. Louis, MO, USA. ²Genome Institute, Washington University School of Medicine, St. Louis, MO, USA. ³Department of Microbiology and Immunology, University of Oklahoma Health Science Center, Oklahoma City, OK, USA. ⁴EMD Millipore Corporation, Billerica, MA, USA. *Corresponding author. E-mail: bcarreno@dom.wustl.edu

Fig. 1. Vaccine candidate identification and immune monitoring.

(A) Distribution of somatic (exomic and missense) mutations identified in metachronous tumors of patients MEL21 and MEL38 (anatomical location and date of collection indicated) and tumor of patient MEL218. HLA-A*02:01-binding candidate peptides were identified in silico among AASs; expression of genes encoding mutated proteins was determined from cDNA capture data (tables S1 to S3). Venn diagrams show expression, among metachronous tumors, of mutated genes encoding vaccine neoantigens. The identities of the three immunogenic neoantigens identified in each patient are depicted; color coding identifies naturally occurring (red) and vaccine-induced (blue) neoantigens. **(B)** Immune monitoring of neoantigen-specific CD8⁺ T cell responses. Results are derived from PBMCs isolated before dendritic cell vaccination (prevaccine) and at peak (postvaccine). PBMCs were cultured in vitro in the presence of peptide and IL-2 for 10 days, followed by HLA-A*02:01/AAS-peptide dextramer assay. This immune monitoring strategy allows the reliable detection as well as the assessment of replicative potential of vaccine-induced T cell responses (fig. S4A). Color coding is same as in (A); numbers within dot plots represent percent neoantigen-specific T cells in lymph⁺/CD8⁺ gated cells.



revealed vaccine-induced T cell immunity to two additional neoantigens per patient: TKT R438W and CDKN2A E153K (55% and 12%, respectively) in patient MEL21; AKAP13 Q285K and OR8B3 T190I (47% and 42%, respectively) in patient MEL38, and MRPS5 P59L and PABPC1 R520Q (58% and 84%, respectively) in patient MEL218 (Fig. 1B). Two of the three patients, MEL21 and MEL218, had preexisting immunity to G209-2M and G280-9V peptides, as determined by the presence of gp100-specific T cells in prevaccine PBMC samples and their ex vivo expansion upon antigen stimulation (fig. S5B). Upon vaccination, these T cell responses were enhanced in patients MEL21 and MEL218 and revealed in patient MEL38 (fig. S5). No T cell immunity to the remaining 12 AAS peptides was detected. Overall, robust neoantigen T cell immunity was detectable as early as week 2 and peaked at week 8 to 9 after the initial vaccine dose (fig. S4A). Neoantigen-specific CD8⁺ T cells were readily identified by dextramer assay directly in postvaccine PBMC samples (fig. S4B) and memory T cells were detected up to 4 months after the final vaccine dose.

Analysis of T cell reactivity among the three patients indicated no preferential skewing toward AAS at specific positions in the peptide sequence—that is, toward TCR contact residues or primary anchor residues (13). Rather, in each patient, T cell immunity appeared to focus on the three AAS candidates exhibiting the highest HLA-A*02:01 binding affinity, whereas the remaining medium- to high-affinity peptides were nonimmunogenic (table S4) (8, 11). Immunogenic AAS peptides (Fig. 1A) were not preferentially derived from

genes with high allelic frequency or expression levels (tables S1 to S3).

To characterize the function of vaccine-induced neoantigen-specific T cells, we established short-term expanded CD8⁺ T cell lines and confirmed their antigen specificity by dextramer assay (fig. S4B) (7, 12). Neoantigen-specific T cells displayed significant levels of cytotoxic activity at AAS peptide concentrations of 1 to 10 nM, a finding that is consistent with high-avidity T cell recognition of antigen (Fig. 2A). OR8B3 T190I-specific T cells could not discriminate between AAS and wild-type peptide when presented on T2 cells, whereas all of the remaining T cell lines showed clear specificity for AAS peptide sequences (Fig. 2A). Next, we sought to characterize the cytokine production profile of these T cells, as a previous report suggests that IL-12p70-producing dendritic cells promote type 1 CD8⁺ T immunity, which in turn correlates with increased clinical benefit (7, 14). Upon antigen stimulation, most vaccine-induced neoantigen-specific T cells produced high amounts of IFN- γ relative to IL-4, IL-5, and IL-13—a pattern that is indicative of a type 1 phenotype (fig. S6). However, SEC24A P469L-specific T cells exhibited a type 2-skewed phenotype (high IL-4, IL-5, and IL-13 levels relative to IFN- γ), and TMEM48 F169L-specific T cells showed a mixed phenotype (high IL-13 levels, but not higher IL-4 or IL-5 levels, relative to IFN- γ) (fig. S6).

We next transfected DM6, a HLA-A*02:01⁺ melanoma cell line (15), with tandem minigene constructs (TMCs) to evaluate neoantigen processing and presentation. Each minigene encoded an AAS, or the corresponding wild-type amino

acid, embedded in 19 to 21 amino acids derived from the normal gene product (fig. S7A and table S5). TMCs also encoded the West Nile virus (WNV) SVG9 (16) and melanoma G280 (17) antigenic determinants as controls (figs. S5 and S7B). Seven of the nine immunogenic neoantigens—TMEM48 F169L, TKT R438W, CDKN2A E153K, SEC24A P469L, AKAP13 Q285K, EXOC8 Q656P, and PABPC1 R520Q—were processed and presented, as evidenced by cytotoxic activity (Fig. 2B) and IFN- γ production (fig. S7C) by corresponding neoantigen-specific T cells upon coculture with DM6 cells expressing AAS-encoding TMCs (AAS-TMCs). In contrast, neither cytotoxic activity (Fig. 2B) nor IFN- γ production (fig. S7C) was observed upon coculture of OR8B3 T190I- and MRPS5 P59L-specific T cells with DM6 cells expressing AAS-TMCs; this finding suggests that these neoantigens are not processed and presented from endogenously expressed protein. None of the neoantigen-specific T cells recognized wild type-encoding TMCs (Fig. 2B and fig. S7C).

On the basis of these findings and the immune monitoring results (Fig. 1B), the nine neoantigens identified in this study fall into three distinct antigenic determinant categories (18, 19). TMEM48 F169L, SEC24A P469L, and EXOC8 Q656P represent dominant antigens, as T cell immunity was detected prior to vaccination (naturally occurring) (Fig. 1B) and these neoantigens were processed and presented from endogenously expressed protein (Fig. 2B). TKT R438W, CDKN2A E153K, AKAP13 Q285K, and PABPC1 R520Q are characterized as subdominant antigens, as T cell immunity required peptide vaccination (Fig. 1B) and

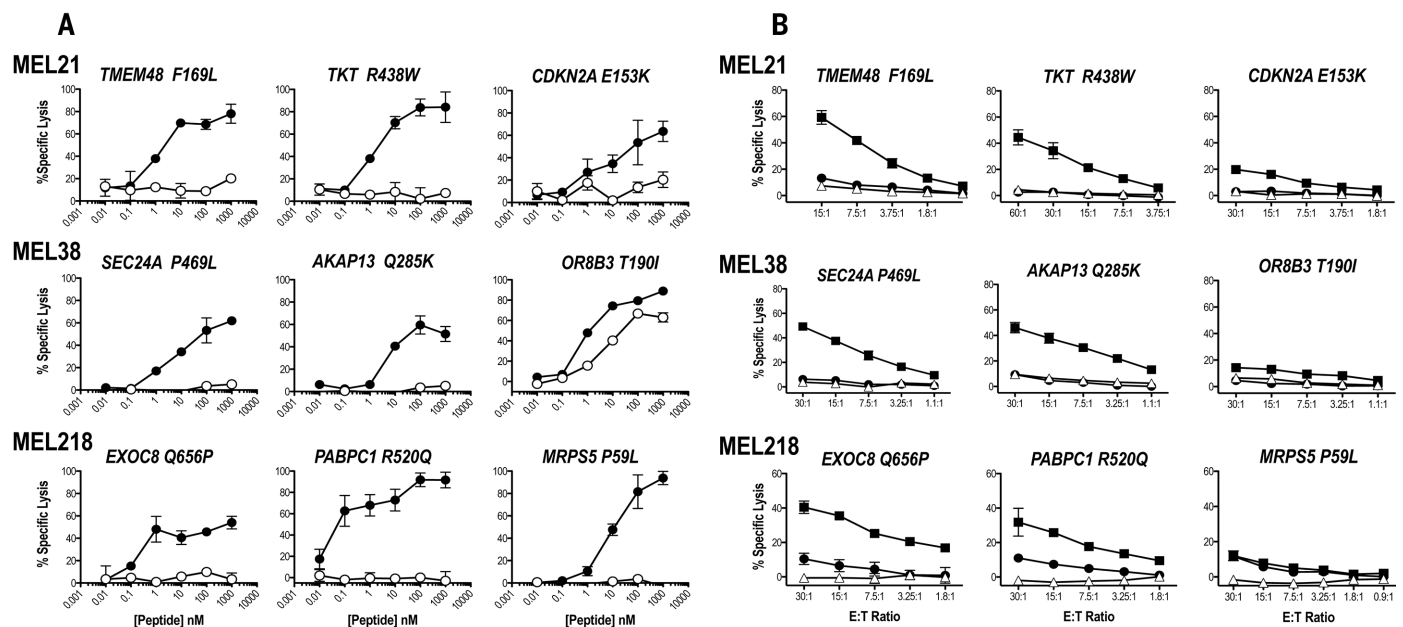


Fig. 2. Antigenic determinants recognized by vaccine-induced T cells.

(A) Neoantigen-specific T cells recognition of AAS (solid circles) and wild-type peptides (open circles) was determined in a standard 4-hour ⁵¹Cr release assay using peptide titrations on T2 (HLA-A*02:01) cells. Percent specific lysis of triplicates (mean ± SD) is shown for each peptide concentration; spontaneous lysis was <5%. Results are shown at E:T ratios of 10:1 for all T cell lines except TMEM48 F169L and CDKN2A E153K T cells (both at 60:1). A repre-

sentative experiment of two independent evaluations is shown. (B) Neoantigen processing and presentation. Neoantigen-specific T cells were cocultured with DM6 cells expressing AAS-encoding TMCs (solid rectangles) or wild type-encoding TMCs (solid circles) in a 4-hour ⁵¹Cr release assay. Open triangles represent lysis obtained with parental DM6 cells. Percent specific lysis of triplicates (mean ± SD) is shown for each E:T ratio; spontaneous lysis was <5%. A representative experiment of two independent evaluations is shown.

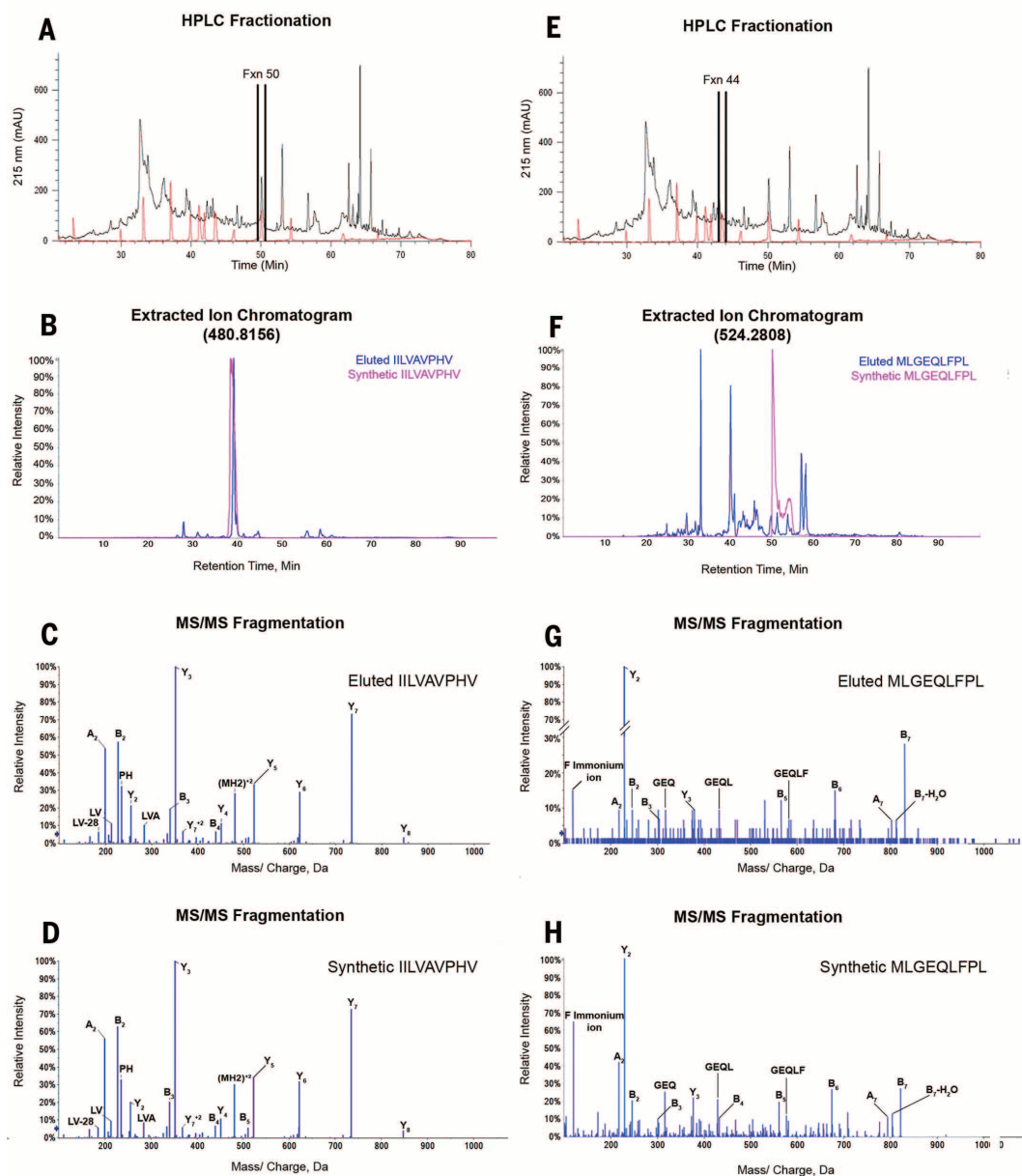


Fig. 3. Processing and presentation of tumor neoantigens. (A) RP-HPLC fractionation of HLA-A*02:01 peptides eluted from the AAS-TMC-expressing melanoma cell line (black trace) and the synthetic peptide mixture containing MEL218 neoantigen candidates (red trace), with fraction 50 indicated. (B) Extracted ion chromatogram of the parent ion with the theoretical mass/charge ratio (m/z) of 480.8156 (+2) in HPLC fraction 50 from the HLA-A*02:01 eluted peptides (blue) overlaid with the EXOC8 Q656P synthetic peptide (pink). (C and D) MS/MS fragmentation pattern of the EXOC8 Q656P ion

eluted from HLA-A*02:01 identified as IILVAVPHV (C) and the corresponding synthetic peptide (D). (E) Same as in (A), with fraction 44 indicated. (F) Extracted ion chromatogram of the parent ion with the theoretical m/z of 524.2808 (+2) in HPLC fraction 44 from the HLA-A*02:01 eluted peptides (blue) overlaid with the PABPC1 R520Q synthetic peptide (pink). (G and H) MS/MS fragmentation pattern of the PABPC1 R520Q ion eluted from HLA-A*02:01 identified as MLGEQLFPL (G) and the corresponding synthetic peptide (H).

these neoantigens were processed and presented from endogenously expressed protein (Fig. 2B). Finally, OR8B3 T190I and MRPS5 P59L constitute cryptic antigens, because peptide vaccination elicited T cell immunity even though these neoantigens were not processed from endogenously expressed protein.

To validate neoantigen processing and presentation, we performed proteomic analysis on peptides eluted from soluble HLA-A*02:01 mol-

ecules isolated from melanoma cells expressing a TMC encoding AAS candidates from a tumor of patient MEL218 (18, 19). Reverse-phase high-performance liquid chromatography (RP-HPLC) was used to reduce the complexity and determine the elution profile of the pool of soluble HLA-A*02:01-restricted peptides presented by melanoma cells, as well as the synthetic AAS peptide mixture (Fig. 3, A and E). The fractions corresponding to each synthetic peptide were subjected

to nanoscale liquid chromatography–mass spectrometry (nano LC/MS). Extracted ion chromatograms revealed the presence of an eluted peptide with a retention time within 2 min of synthetic EXOC8 Q656P peptide in fraction 50 (Fig. 3B). MS/MS fragmentation pattern comparison of the eluted and synthetic peptides ensured EXOC8 Q656P sequence identity and confirmed HLA-A*02:01 presentation of this dominant neoantigen (Fig. 3, C and D). A similar analysis of fraction 44

8. M. Nielsen *et al.*, *Protein Sci.* **12**, 1007–1017 (2003).
9. C. R. Cabanski *et al.*, *J. Mol. Diagn.* **16**, 440–451 (2014).
10. J. Elvin, C. Potter, T. Elliott, V. Cerundolo, A. Townsend, *J. Immunol. Methods* **158**, 161–171 (1993).
11. R. Buchli *et al.*, *Biochemistry* **44**, 12491–12507 (2005).
12. B. M. Carreno *et al.*, *J. Immunol.* **188**, 5839–5849 (2012).
13. Y. Kim, A. Sette, B. Peters, *J. Immunol. Methods* **374**, 62–69 (2011).
14. W. H. Fridman, F. Pagès, C. Sautès-Fridman, J. Galon, *Nat. Rev. Cancer* **12**, 298–306 (2012).
15. T. L. Darrow, C. L. Slingluff Jr., H. F. Seigler, *J. Immunol.* **142**, 3329–3335 (1989).
16. C. P. McMurtrey *et al.*, *Proc. Natl. Acad. Sci. U.S.A.* **105**, 2981–2986 (2008).
17. A. L. Cox *et al.*, *Science* **264**, 716–719 (1994).
18. E. E. Sercarz *et al.*, *Annu. Rev. Immunol.* **11**, 729–766 (1993).
19. E. Assarsson *et al.*, *J. Immunol.* **178**, 7890–7901 (2007).
20. A. Gros *et al.*, *J. Clin. Invest.* **124**, 2246–2259 (2014).
21. E. Tran *et al.*, *Science* **344**, 641–645 (2014).
22. H. Robins *et al.*, *J. Immunol. Methods* **375**, 14–19 (2012).
23. A. Lossius *et al.*, *Eur. J. Immunol.* **44**, 3439–3452 (2014).
24. H. S. Robins *et al.*, *Sci. Transl. Med.* **5**, 214ra169 (2013).
25. P. G. Coulie, B. J. Van den Eynde, P. van der Bruggen, T. Boon, *Nat. Rev. Cancer* **14**, 135–146 (2014).
26. M. Gerlinger *et al.*, *Annu. Rev. Genet.* **48**, 215–236 (2014).
27. H. Shi *et al.*, *Cancer Discov.* **4**, 80–93 (2014).
28. E. M. Van Allen *et al.*, *Cancer Discov.* **4**, 94–109 (2014).
29. E. Cha *et al.*, *Sci. Transl. Med.* **6**, 238ra70 (2014).
30. M. Rajasagi *et al.*, *Blood* **124**, 453–462 (2014).

ACKNOWLEDGMENTS

We thank T. Hansen, D. Link, and J. DiPersio for critical review; T. Ley, M. Walter, and J. Welch for advice and helpful discussions; R. Austin, R. Demeter, W. Eades, S. McGrath, W. Swaney, T. Vickery, J. Walker, and T. Wylie for technical assistance; L. Cornelius, R. Fields, R. Aft, J. Moley, A. Schaffer, and J. Steel for clinical collaboration; A. Alyasiry, S. Kalathiveetil, I. King, M. Schellhardt, and C. Rush for clinical research support; and B. Fritz from Adaptive Biotechnologies for technical guidance. Supported by Barnes-Jewish Hospital Foundation, Siteman Cancer Frontier Fund, Our Mark on Melanoma (MOM) Foundation, Come Out Swinging (COS) Foundation, Blackout Melanoma Foundation, and National Cancer Institute grants P30 CA91842 and R21 CA179695 (B. Carreno, PI). We acknowledge the Genome Institute at Washington University School of Medicine for the sequencing production pipeline that generated data, established by National Human Genome Research Institute grant 5U54HG003007 (R. Wilson, PI). The Siteman Cancer Center provided the use of the Flow Cytometry Core, Clinical Trials Core, Tissue Procurement Core, and Biologic Therapy Core. The data presented in this manuscript are tabulated in the main paper and the supplementary materials. The raw exome and transcriptome sequence data are available on the Sequence Read Archive database: Bioproject PRJNA278450. The raw proteomic data are available at MassIVE database ID MSV000079125. Washington University and the authors (B.M.C., V.M., E.R.M., and G.P.L.) have filed a patent application (US62/050,195) related to the use of tumor somatic mutations for cancer immunotherapy entitled “Cancer Immunotherapy, Methods, Compositions and Uses Thereof.” We thank the patients and families for their dedicated participation in this study.

SUPPLEMENTARY MATERIALS

www.sciencemag.org/content/348/6236/803/suppl/DC1
Materials and Methods
Supplementary Text
Figs. S1 to S10
Tables S1 to S10
References (31–36)

26 November 2014; accepted 19 March 2015
Published online 2 April 2015;
10.1126/science.aaa3828

CENTROSOMES

Regulated assembly of a supramolecular centrosome scaffold in vitro

Jeffrey B. Woodruff,^{1*} Oliver Wueseke,^{1*} Valeria Viscardi,² Julia Mahamid,³ Stacy D. Ochoa,² Jakob Bunkenborg,^{4,5} Per O. Widlund,^{1†} Andrei Pozniakovsky,¹ Esther Zanin,^{2‡} Shirin Bahmanyar,^{2§} Andrea Zinke,¹ Sun Hae Hong,⁶ Marcus Decker,^{1||} Wolfgang Baumeister,³ Jens S. Andersen,⁵ Karen Oegema,^{2¶} Anthony A. Hyman^{1¶¶}

The centrosome organizes microtubule arrays within animal cells and comprises two centrioles surrounded by an amorphous protein mass called the pericentriolar material (PCM). Despite the importance of centrosomes as microtubule-organizing centers, the mechanism and regulation of PCM assembly are not well understood. In *Caenorhabditis elegans*, PCM assembly requires the coiled-coil protein SPD-5. We found that recombinant SPD-5 could polymerize to form micrometer-sized porous networks in vitro. Network assembly was accelerated by two conserved regulators that control PCM assembly in vivo, Polo-like kinase-1 and SPD-2/Cep192. Only the assembled SPD-5 networks, and not unassembled SPD-5 protein, functioned as a scaffold for other PCM proteins. Thus, PCM size and binding capacity emerge from the regulated polymerization of one coiled-coil protein to form a porous network.

Pericentriolar material (PCM), a matrix of proteins that regulates microtubule nucleation, anchoring, and dynamics (1, 2), assembles around centrioles to form centrosomes that contribute to cell division. The PCM scaffold is thought to form via the assembly of coiled-coil proteins [pericentrin and Cdk5RAP2/centrosomin in vertebrates and *Drosophila*, and SPD-5 in *Caenorhabditis elegans* (3–8)]. PCM expansion during mitotic entry requires SPD-2/Cep192 and is regulated by mitotic kinases, including the Polo family kinase Plk1 (9–13). However, the mechanism of PCM assembly remains unclear, partly due to the lack of an in vitro system.

In *C. elegans*, PCM assembly requires SPD-5, a protein with nine predicted coiled-coil domains (Fig. 1A) (7). Because coiled-coil domains often mediate homo-oligomerization (14), we hypothesized that SPD-5 self-association could underlie PCM assembly. To test this idea, we purified full-

length, green fluorescent protein (GFP)-labeled SPD-5 (SPD-5::GFP) from baculovirus-infected insect cells (Fig. 1, A and B) (fig. S1A shows all proteins used in this study). Using total internal reflection microscopy to count GFP moieties in SPD-5::GFP particles by photobleaching revealed that SPD-5::GFP initially exists as monomers and dimers (Fig. 1C), consistent with in vivo data (15). To determine whether SPD-5 could form larger assemblies, we shifted SPD-5::GFP from ice to 23°C and observed samples using widefield fluorescence microscopy. After 120 min, 25 nM SPD-5::GFP assembled into dense structures spanning several micrometers that we term “networks” (Fig. 1D); similar assemblies were observed by phase contrast microscopy using untagged SPD-5 (fig. S1B). Network formation decreased with lower initial SPD-5::GFP concentrations (Fig. 1D). Temporal analysis using 25 nM SPD-5::GFP revealed single puncta that grew into extended meshworks (Fig. 1E); separate networks could also be observed coalescing during assembly (fig. S1C). SPD-5 networks readily dissolved after dilution or mechanical disruption, indicating that network formation is reversible (fig. S1D).

We calculated total SPD-5 network mass per sample by summing the integrated fluorescence intensity of all SPD-5::GFP networks (up to 200,000 per sample) in the imaged area (Fig. 1F). We also calculated the size distribution of the networks in each sample (fig. S1E). The kinetics of SPD-5::GFP network formation fit a sigmoidal curve typical of growing polymers, including a characteristic lag time and plateau (Fig. 1F). Thus, SPD-5 alone can polymerize in vitro in a concentration and time-dependent manner to form extended networks that reach sizes comparable to fully expanded PCM in vivo (11). Low-magnification cryo-electron microscopy of SPD-5 networks revealed dense, amorphous assemblies interspersed

¹Max Planck Institute of Molecular Cell Biology and Genetics, Pflotenhauserstrasse 108, 01307 Dresden, Germany.

²Department of Cellular and Molecular Medicine, Ludwig Institute for Cancer Research, University of California, San Diego, La Jolla, CA 92093, USA. ³Department of Molecular Structural Biology, Max Planck Institute of Biochemistry, Martinsried 82152, Germany. ⁴Department of Clinical Biochemistry, Copenhagen University Hospital, Hvidovre 2650, Denmark. ⁵Department of Biochemistry and Molecular Biology, University of Southern Denmark, Odense, Denmark. ⁶Department of Molecular and Cell Biology, University of California, Berkeley, Berkeley, CA 94720, USA.

*These authors contributed equally to this work. †Present address: Department of Chemistry and Molecular Biology, University of Gothenburg, Medicinargatan 9 c, 40530 Gothenburg, Sweden ‡Present address: Department of Biology II, Cell and Developmental Biology, Ludwig-Maximilians-Universität München, Martinsried, Germany §Present address: Department of Molecular, Cell, and Developmental Biology, Yale University, 219 Prospect St., New Haven, CT 06520, USA ||Present address: Department of Research Oncology, Genentech, 1 DNA Way South San Francisco, CA 94080, USA. ¶Corresponding author. E-mail: hyman@mpi-cbg.de (A.A.H.); koegema@ucsd.edu (K.O.)